

Supplementary Data

Nuclear receptors connect progenitor transcription factors to cell cycle control.

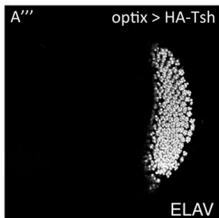
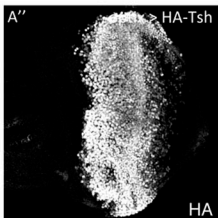
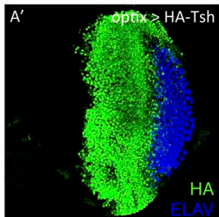
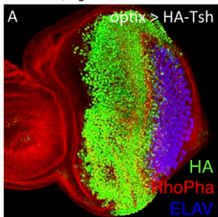
Marta Neto^{1,3}, Marina Naval-Sánchez², Delphine Potier², Paulo S. Pereira³, Dirk Geerts⁴, Stein Aerts^{2*}, Fernando Casares^{1*}

- 1- CABD, Andalusian Centre for Developmental Biology, CSIC-UPO-JA, 41013 Seville, SPAIN.
- 2- School of Medicine, University of Leuven, box 602 3000 Leuven, BELGIUM.
- 3- IBMC/Instituto de Investigação e Inovação em Saúde, Universidade do Porto, 4200-135 Porto, PORTUGAL.
- 4- Department of Pediatric Oncology. Erasmus University Medical Center, 3015 CN Rotterdam, THE NETHERLANDS.

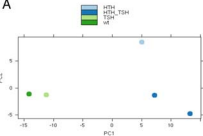
(*) Contacts: Stein.Aerts@med.kuleuven.be; fcasfer@upo.es

Contains:

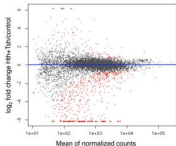
- Supplementary Figures S1-10
- Supplementary Table S4
- Legends to Supplementary data (Figures S1-10; Tables S1-7)



A



B



C

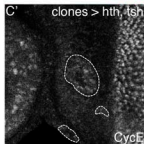
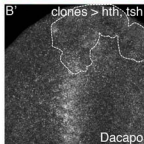
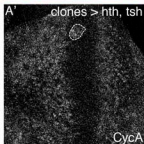
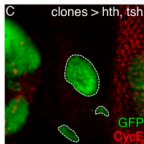
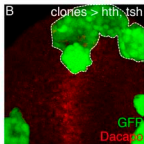
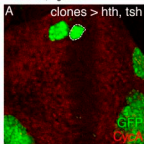
Hth+Tsh down-regulated genes

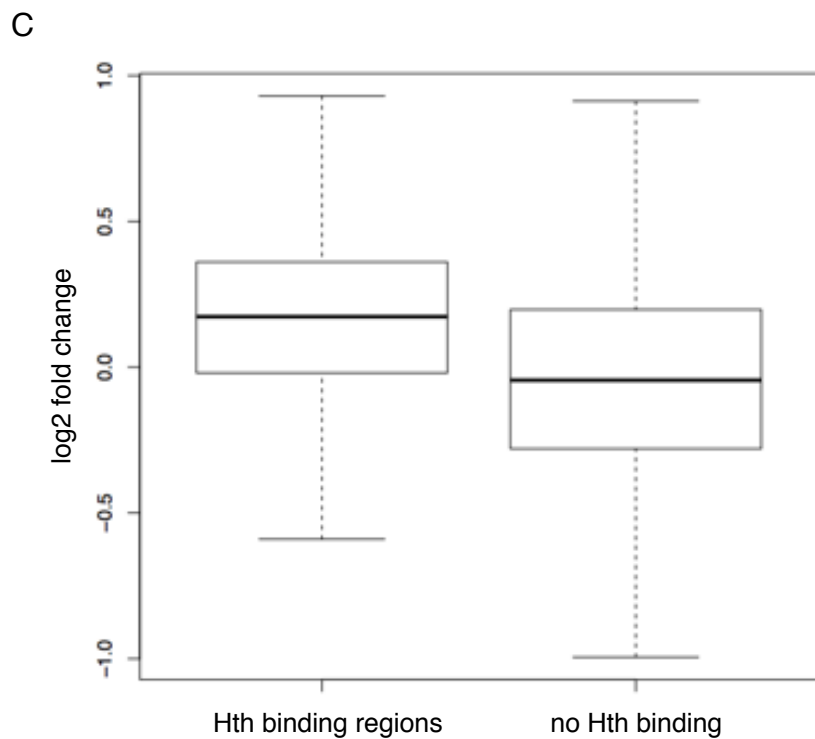
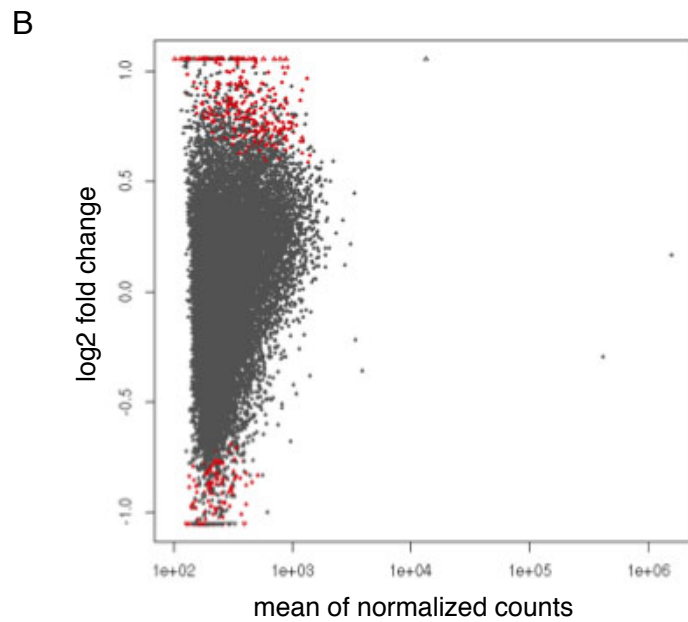
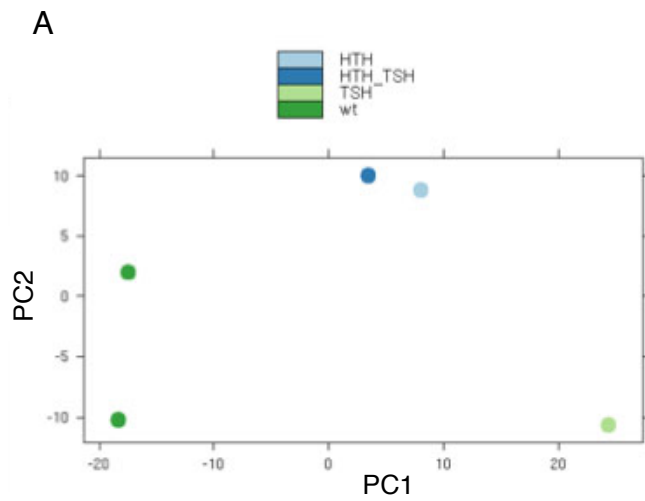
| Gene Ontology Term | P-adjusted |
|--|------------|
| <i>Generation of neurons</i> | 2.23E-28 |
| <i>Nervous system development</i> | 2.98E-21 |
| <i>Signaling</i> | 6.31E-21 |
| <i>Cell communication</i> | 1.78E-20 |
| <i>System development</i> | 3.87E-19 |
| <i>Axon development</i> | 8.49E-19 |
| <i>Anatomical structure morphogenesis</i> | 6.08E-18 |
| <i>Compound eye photoreceptor cell differentiation</i> | 3.40E-17 |
| <i>Cell projection organization</i> | 9.85E-17 |

D

Hth+Tsh up-regulated genes

| Gene Ontology Term | P-adjusted |
|---|------------|
| <i>DNA-dependent DNA replication</i> | 5.82E-14 |
| <i>DNA metabolic process</i> | 1.13E-07 |
| <i>Nuclear cell cycle DNA replication</i> | 2.93E-07 |
| <i>Cell cycle</i> | 3.05E-05 |
| <i>Single organism organelle organization</i> | 8.82E-05 |
| <i>Mitotic cell cycle process</i> | 0.00048 |
| <i>Pyrimidine deoxyribonucleotide metabolic process</i> | 0.00137 |
| <i>Cytoskeleton organization</i> | 0.00191 |
| <i>Meiotic cell cycle process</i> | 0.00241 |

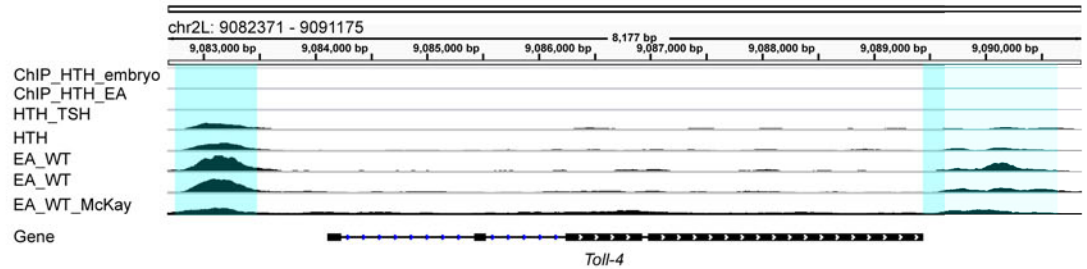




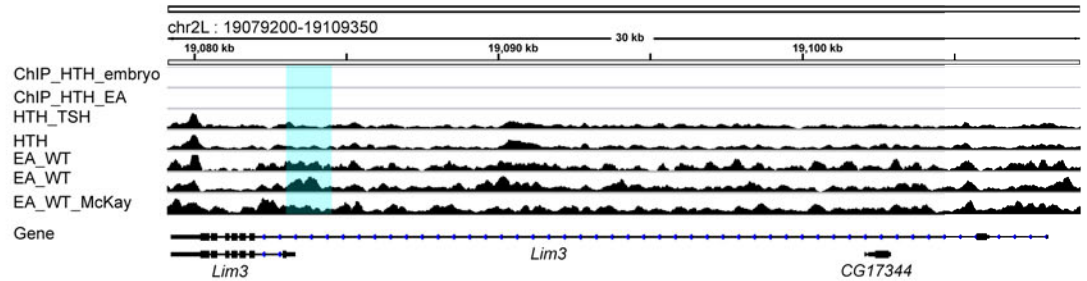
D 1. 



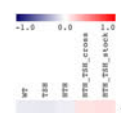
2.



3.

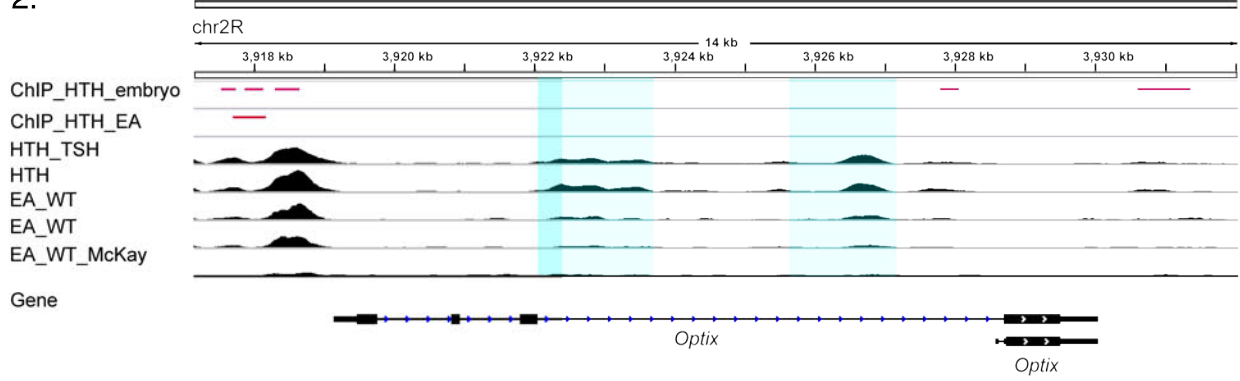


E1.

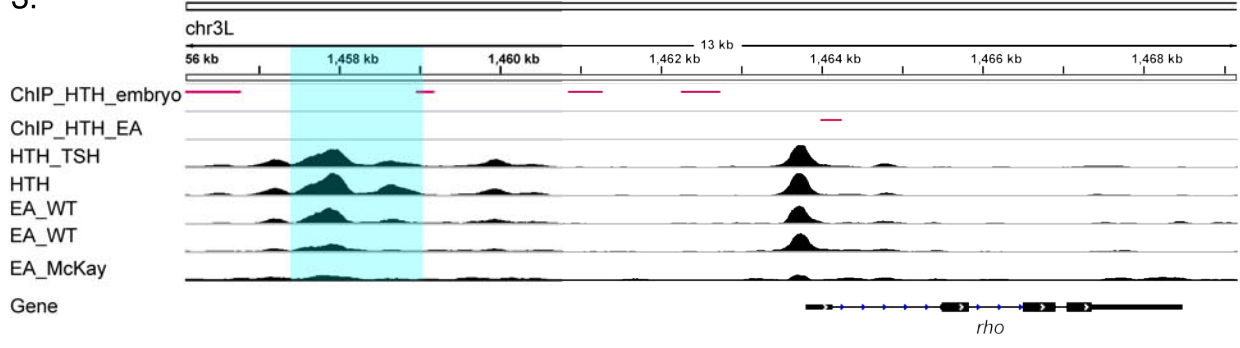


- Eip74EF
- CG3835
- Optix
- Eaf6
- CG18259
- px
- CG10428
- so
- CG11145
- lt
- RhoGAP71E
- RpLP2
- RpS15
- CG12304
- CG32164
- sea
- CG3964
- CG8317
- mrn
- CG12301
- vfl
- Ser
- tna
- CG7656
- Cdk4
- hth
- mab-21
- CG30283
- CG4788
- CG6900
- Notum
- esn
- m2
- CG16979
- Eip78C
- CG5065
- Hr46
- Blimp-1
- nkd
- Clbn
- klar
- CG17838
- boi
- HLHm3
- ph-p
- CG33144
- Hdc
- ed
- Sobp
- sens-2
- bbg
- CG2556
- luna
- Pka-R1
- dpr
- CG9134
- rho
- CG8213
- dpr12
- CG9896
- CG33232
- CG6498
- G-alpha47A
- Fs
- CG8311
- Mur2B
- CG4927
- CG10898
- CG42747
- CG6018
- kek5
- CG8306
- vn
- ex
- fng
- Tsp
- Egfr
- sbb
- tai
- jing
- shn
- CASK
- kibra
- ft
- N
- Snoo
- grn
- CG6398
- CG8303
- mld
- ImpL2
- dve
- Dl
- Lim1
- dlp
- grh
- br
- lbk
- hig
- ImpE1
- sli

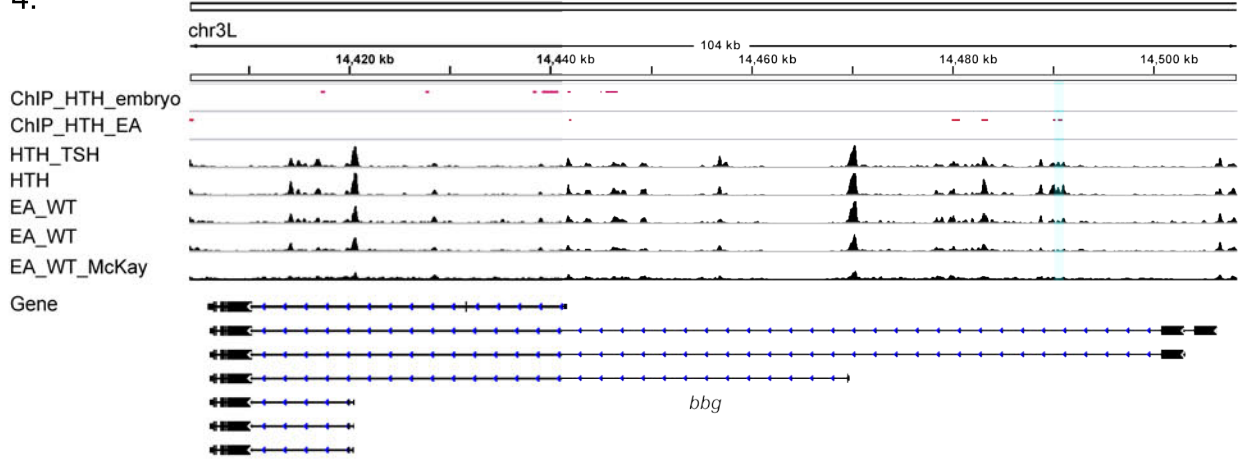
2.



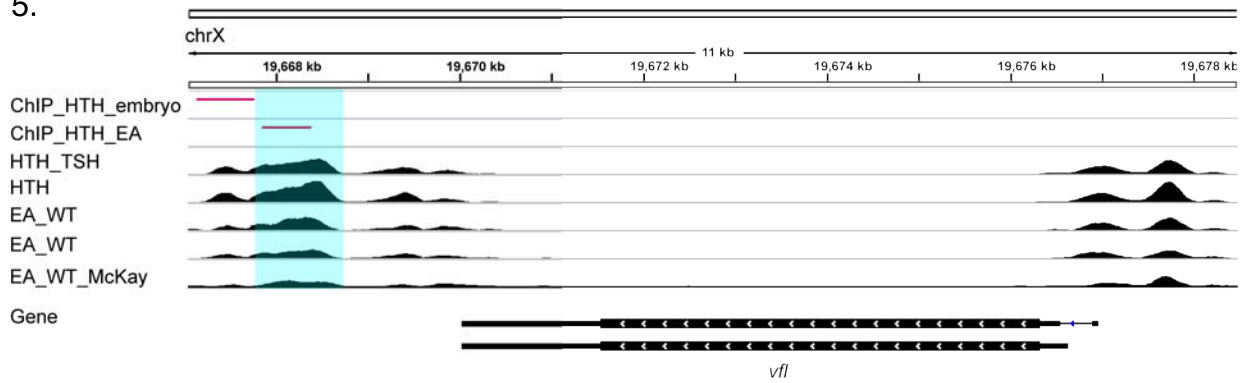
3.



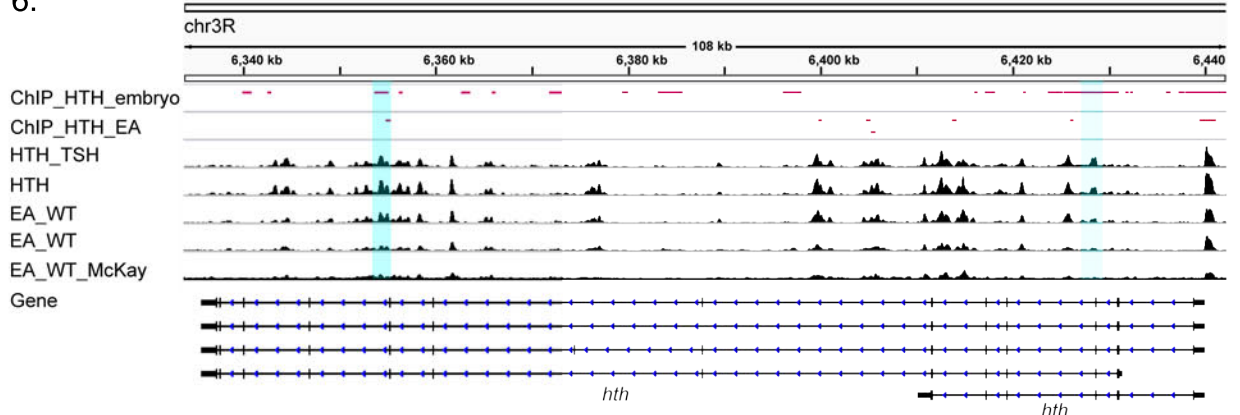
4.









5.



6.



Neto et al., Figure S5

| Cluster Rank | NES | Best motif logo | Best motif name | Candidate TFs |
|--------------|-----|---|------------------------|---------------|
| 1 | 7.4 |  | jaspar-PF0001.1 | ewg |
| 4 | 4.9 |  | selexconsensus-EcR_usp | EcR |
| 6 | 4.8 |  | transfac_public-M00027 | sd |
| 9 | 4.4 |  | homer-M00191 | Stat92E |
| 18 | 3.9 |  | transfac_pro-M00920 | E2f, E2f2, Dp |
| 21 | 3.8 |  | transfac_pro-M01345 | so, Optix |

+bcd + ATF3 +Adf1 +slbo +oc +MAd +DNApoliota +gem + pnr

UASDHR3RNA*(8)* (412)UASDHR3RNA*(8)* (413)

UASDHR4RNA (12044)

UASDHR4RNA (20157)

UASDHR4RNA (306837)

UAS 5-DHR3 (ii)

UAS 5-DHR3 (iii)



UAS DHR3 RB (i)

UASDHR4-T1RNA (10625)

UASDHR4-T1RNA (104403)

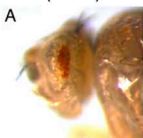
UASDHR4-T1RNA (2958)

UASDHR4-T1

UASDHR4-T1

UAS EvRR1

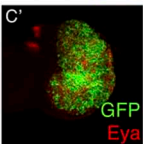
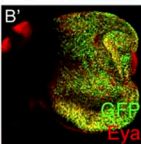
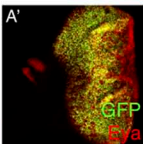
UASftz-f1RNAi
(33625)



UASftz-f1RNAi
(2959)



UASalphaftz-f1



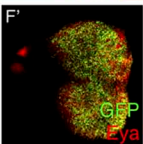
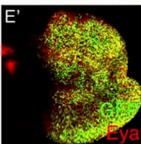
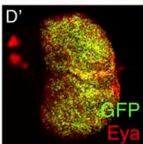
UASDHR3RNAi
(II) (412)



UASDHR3RNAi
(III) (413)



UASHr46RNAi
(20157)



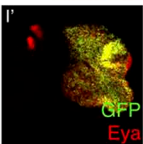
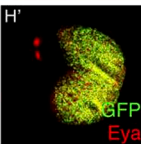
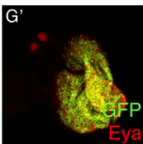
UASHr46RNAi
(106837)

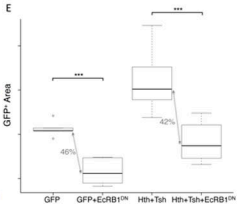
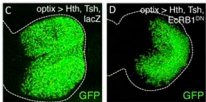
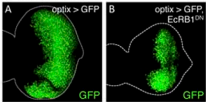


UAS S-DHR3
(II)

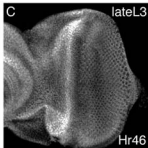
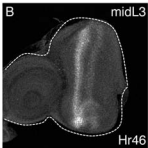
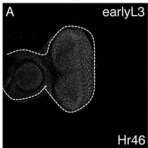


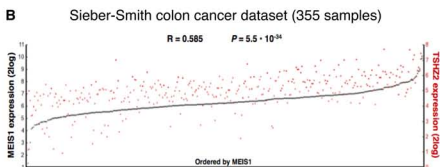
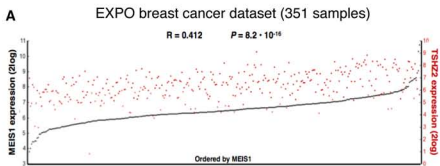
UAS S-DHR3
(III)



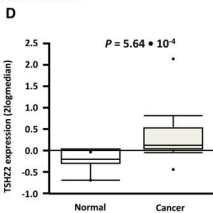
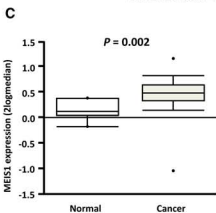


Neto et al., Figure S9





Finak breast cancer dataset



TCGA-2 colon cancer dataset

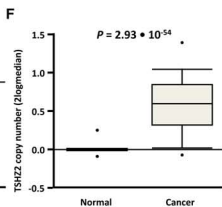
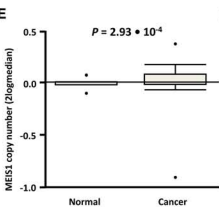


Figure Legends

Supplementary Figure 1. The *optix2/3-GAL4* line (“*optix>*”) drives expression in undifferentiated cells anterior to the morphogenetic furrow (MF). *optix2/3-GAL4*; *UAS-HA:tsh* (“*optix>HA:tsh*”) L3 eye disc, stained for actin (Rhodamine-phalloidin, to outline tissue shape, red), HA, which tags *tsh* (green) and the photoreceptor marker Elav (blue). Anterior is to the left. Most of the HA:tsh driven by *optix2/3-GAL4* is detected anterior to the MF (line in A).

Supplementary Figure 2. (A) Principal Component analysis of the RNA-seq data from the five samples used. The analysis highlights the similarity of *optix>tsh* (“TSH”) to the control, *optix>GFP* (“WT”), and between the two *optix>hth+tsh* biological replicates. *optix>hth* stands out as a different set. (B) MA-plot representing the log₂ fold gene expression change of *optix>hth+tsh* over *optix>GFP* (“control”) (y-axis), versus the abundance (x-axis). Red dots are differentially expressed genes. (C,D) Selected GO terms associated to genes that are down-regulated (C) or up-regulated (D) in *optix>hth+tsh* compared to the control *optix>GFP*.

Supplementary Figure 3. Co-expression of *hth+tsh* regulates the expression of cell cycle-related genes. GFP-marked clones overexpressing *hth+tsh* were induced in the eye imaginal disc at 48-72 hours after egg laying. Discs are stained with (A,A') anti-CycA, (B,B') anti-Dacapo and (C-C') anti-CycE (red). *hth+tsh*-expressing clones activate CycA and CycE expression and repress the expression of Dacapo.

Supplementary Figure 4. (A) Principal Component analysis of the FAIRE-seq data from the five samples used. (B) MA-plot representing the log₂ fold gene expression change of *optix>hth+tsh* over control (y-axis), versus the abundance (x-axis). Red dots are differentially open peaks. (C) Association of FAIRE peaks (with or without Hth binding) to gene expression. (D1) Heatmap showing RNA-seq results for genes that show significantly closed FAIRE peaks and (D2, D3) genomic view of two examples. (E1) Heatmap showing RNA-seq results for genes that show significantly open FAIRE peaks and (E2 – E6) genomic view of five examples.

Supplementary Figure 5. i-cis-Target predicted transcription factor binding site motifs located within FAIRE peaks with increased accessibility in *optix>hth+tsh* discs.

Supplementary Figure 6. Adult phenotypes produced by the overexpression or RNAi-mediated attenuation of *Hr46/DHR3* and *ftz-f1*. Lateral and dorsal views of adult heads expressing different UAS lines using the *optix2.3-GAL4* line: *DHR3RNAi* #412(A,A'), *DHR3RNAi* #413 (B,B'), *Hr46RNAi* #12044 (C,C'), *Hr46RNAi* #20157 (D,D'), *Hr46RNAi* #106837 (E,E'), *S-DHR3(II)* (F,F'), *S-DHR3(III)* (G,G'), *DHR3 RB* (H,H'), *ftz-f1RNAi* #33625 (I,I'), *ftz-f1RNAi* #104463 (J,J'), *ftz-f1RNAi* #2959 (K,K'), α *ftz-f1* (L,L'), β *ftz-f1* (M,M'), *EcRB1* (N,N').

Supplementary Figure 7. Functional interaction of *hth+tsh* with *Hr46* and *ftz-f1*. Adult (upper panels) and eye disc (lower panels) phenotypes of *optix>hth+tsh+X*, with X being the UAS constructs indicated. Representative cases are shown.

Supplementary Figure 8. The dominant negative form of *EcRB1* partially rescues the *hth+tsh*-phenotype. Late third instar eye discs from (A) *optix>GFP*, (B) *optix>GFP+EcRB1DN*, (C) *optix>hth+tsh+lacZ* or (D) *optix>hth+tsh+EcRB1DN* expressing flies. GFP in (A,B) comes from the UAS-GFP line and in (C,D) from the UAS-131-GFP_{hth} line. The dashed lines outline the discs. (E) Statistical analysis of the GFP-positive area in the different genotypes.

Supplementary Figure 9. Temporal expression of *Hr46*. *Hr46* expression during L3 development in the eye-antennal imaginal disc. Control disc at different developmental stages (early L3 (A), mid L3 (B) and late L3 (C)) stained with anti-*Hr46*. In (A) and (B) the dashed line outlines the disc.

Supplementary Figure 10. Visual representation of *MEIS1* and *TSHZ2* mRNA expression in (A) all 351 samples of the EXPO breast cancer dataset and (B) all 355 samples of the Sieber-Smith colon cancer dataset as analyzed using the R2 website. The tumors are ranked horizontally from left to right according to their *MEIS1* expression as determined by Affymetrix array analyses (2log values). *MEIS1* and *TSHZ2* expression values for each tumor are visualized with black circles and red rectangles, respectively. Dark and light colors denote samples with significant ("present call"), and absent expression, respectively. mRNA expression correlations were calculated with a 2log Pearson test. Full details are in Supplementary Table 4. Visual representation of *MEIS1* (C) and *TSHZ2* (D) mRNA expression in the Finak breast cancer dataset, and *MEIS1* (E) and *TSHZ2* (F) DNA copy number levels in the TCGA-2 colon cancer dataset, as analyzed using the OncoPrint website. Values are

represented as 2log-median centered. *P* values are calculated with a Student's t-test. Full details are in Supplementary Table 5.

Table legends

Supplementary Table 1. Upregulated and downregulated differentially expressed genes in *optix>hth+tsh* discs by RNA-seq.

Supplementary Table 2. FAIRE-seq analysis showing peak location and potential associated genes and *Janelia* lines overlapping peak regions.

Supplementary Table 3. Complete list of RNAi, UAS and dominant negative lines used for testing genetic interactions with *hth+tsh*.

Supplementary Table 4. MEIS1 and TSHZ1-3 mRNA expression and correlation in human cancer datasets.

(A) MEIS1 and TSHZ1-3 mRNA expression in human cancer datasets. Average MAS5.0-normalized data for mRNA expression, with their S.E.M., for the 116 different cancer datasets representing all major cancer types present in the R2 suite, 91 datasets for solid, and 25 for hematopoietic tumors. Only significant expression ("present call" for the probeset in that sample) is counted. Between brackets is the percentage of samples with such a present call. *MEIS1* and *TSHZ1* are almost invariantly well-expressed in solid tumor types, and also *TSHZ2-3* are significantly expressed in the majority of tumor samples. In hematopoietic tumors, *MEIS1* and *TSHZ1-3* are more rarely expressed, and their expression levels are lower, especially *TSHZ2-3*. For comparison: MAS5.0-normalized *GAPDH* and *ACTB* household gene mRNA expression in these datasets ranges between 5,000 and 10,000. (B) MEIS1 and TSHZ1-3 mRNA expression correlations in human cancer datasets. Cancer datasets in R2 with a significant correlation between *MEIS1* and *TSHZ1-3* mRNA expression levels. The number of sets with significant positive and negative expression correlations are listed in the top and bottom rows, respectively. In solid tumor types, MEIS1 is predominantly positively correlated with TSHZ1-3, most notably with TSHZ2-3, in hematopoietic tumors these correlations are also present, but much more infrequent. Complete data are in Supplementary Table 5. Correlations were calculated using a 2log Pearson test, as described in the Materials and Methods. (C) MEIS1 and TSHZ1-3 mRNA over-expression and DNA copy gain in human cancer types. Tumor

types are indicated in the first column. Examples of tumor subtypes with multiple datasets and consistent *MEIS1* and/or *TSHZ1-3* mRNA over-expression and/or DNA copy number gain in the Oncomine website are listed. The number of sets is indicated in the second column, the specific tumor subtypes in the third column. The last four columns list the number of datasets per tumor subtype that show significant mRNA over-expression and/or DNA gain. When in bold type and on a green background, *MEIS1* is also significantly positively correlated with *TSHZ1*, -2, or -3 as analyzed in R2 (Supplementary Table 4). Various * enfolds 4 anaplastic large cell, 2 Burkitt's, 2 follicular, 3 Hodgkin's, 5 large B-cell, and 2 T-cell lymphoma datasets. Complete data are in Supplementary Table 6.

Supplementary Table 5. Complete *MEIS1*-*TSHZ* mRNA co-expression data from the R2 and used for Supplementary Table 3 and Supplementary Figure 10. Tumor type and dataset are listed in the first column, dataset size in the second column. Columns 3-9 show the R values of significant 2logPearson correlation tests for *MEIS1* mRNA expression correlation with the other genes listed. Results are from the probe-set with the highest correlation R value per dataset. Results are only listed if the best probe-set, or at least half of the other probe-sets showed significant correlations. Numbers on green and orange fields signify significant positive and negative correlations, respectively. Grey fields indicate that no probe-set was present. Column 10 lists the GEO GSE number, through which full set data can be obtained at the NCBI GEO website. (*)Available at <http://cancergenome.nih.gov>. (**)Available at <http://www.ebi.ac.uk/arrayexpress>. (***)Combination of GSE datasets 16910/18290/19348/21668. Results in bold red type are used as the examples in Supplementary Figure 10 (A, B).

Supplementary Table 6. Complete *MEIS1* and *TSHZ1-3* mRNA over-expression and DNA copy number gain data from Oncomine used for Supplementary Table 3C and Supplementary Figure 10. Shown are all tumor (sub)types with significant results. Tumor (sub)types with consistent *MEIS1*-*TSHZ* mRNA over-expression and/or DNA copy number gains in multiple datasets are on a green background. Tumor type and subtype are listed in the first two columns. Columns 3-6 show P value of mRNA over-expression (for mRNA datasets) or DNA copy number gain (for DNA datasets) in tumor over (matched) normal tissue, respectively. P values are as determined by a 2log-median centered t-test using the Oncomine default settings. Columns 7-9 show dataset name, type, and size, respectively. Columns 10 and 11 show amount of tumor, and normal tissue samples used in the t-test, respectively. Green fields indicate

consistent results for different datasets with the same tumor (sub)type. Results in bold red type are used as the examples in Supplementary Figure 10 (C-F).

Supplementary Table 7. Overview of MEIS1 co-expression with TSHZ, YAP1, RORA, and NR5A2 genes from R2 data. The first two columns list tumor type and amount of datasets. Columns 3-8 show whether at least half of the datasets showed consistent significant positive (POS; green field) or negative (NEG; orange field) mRNA expression correlations with MEIS1. Statistics and other details are as in Supplementary Table 5.

A

| 116 cancer sets | | | | |
|------------------------------------|-----------------------|-----------------------|----------------------|----------------------|
| | MEIS1 | TSHZ1 | TSHZ2 | TSHZ3 |
| Solid tumors (n=91) | 313 ± 35 (96%) | 268 ± 17 (97%) | 114 ± 7 (54%) | 112 ± 6 (85%) |
| Hematopoietic tumors (n=25) | 294 ± 74 (52%) | 168 ± 14 (74%) | 75 ± 11 (8%) | 76 ± 6 (25%) |

B

| 91 solid cancer sets | | | |
|-----------------------------|-------------|-------------|-------------|
| | MEIS1-TSHZ1 | MEIS1-TSHZ2 | MEIS1-TSHZ3 |
| Significant positive | 46 | 56 | 60 |
| Significant negative | 6 | 2 | 7 |

| 25 hematopoietic cancer sets | | | |
|------------------------------|-------------|-------------|-------------|
| | MEIS1-TSHZ1 | MEIS1-TSHZ2 | MEIS1-TSHZ3 |
| Significant positive | 3 | 8 | 10 |
| Significant negative | 3 | 1 | 4 |

C

| Solid tumor | | | | | | |
|-------------|------|--|-------|-------|-------|-------|
| Tumor type | Sets | Subtype | MEIS1 | TSHZ1 | TSHZ2 | TSHZ3 |
| Bladder | 4 | Bladder urothelial carcinoma | 3 | | 3 | 4 |
| Brain | 16 | Astrocytoma, glioblastoma, oligodendroglioma | 10 | 7 | 7 | 4 |
| Breast | 8 | Breast carcinoma, invasive | 5 | 1 | 4 | 3 |
| Cervix | 3 | Cervical squamous cell carcinoma | 3 | | 3 | 1 |
| Colon | 18 | Colorectal adenocarcinoma | 9 | | 13 | 4 |
| Endometrium | 2 | Endometrial adenocarcinoma | 2 | | 2 | |
| Esophagus | 2 | Esophageal adenocarcinoma | | | | 2 |
| Germ cell | 2 | Teratoma, testicular | 1 | 2 | 1 | 1 |
| Head & Neck | 3 | Head & neck squamous cell carcinoma | 2 | | 2 | 1 |
| Kidney | 5 | Renal cell carcinoma | 1 | | 5 | 1 |
| Liver | 6 | Hepatocellular carcinoma | 4 | 1 | 3 | 3 |
| Lung | 13 | Lung adenocarcinoma, squamous cell carcinoma | 8 | | 12 | 6 |
| Ovary | 7 | Ovarian adenocarcinoma, carcinoma | 7 | | 1 | 1 |
| Pancreas | 5 | Pancreatic adenocarcinoma | 1 | 1 | 4 | 4 |
| Prostate | 2 | Prostate adenocarcinoma | 2 | | 2 | 2 |
| Thyroid | 1 | Thyroid gland papillary carcinoma | 1 | | 1 | 1 |

| Hematopoietic tumor | | | | | | |
|---------------------|------|--------------------------------------|-------|-------|-------|-------|
| Tumor type | Sets | Subtype | MEIS1 | TSHZ1 | TSHZ2 | TSHZ3 |
| Leukemia | 8 | Acute lymphoblastic leukemia | 6 | 6 | 1 | |
| Leukemia | 7 | Acute myeloid leukemia | 7 | 2 | | 1 |
| Lymphoma | 18 | Various * | 17 | 5 | 5 | 13 |
| Myeloma | 2 | Multiple myeloma, smoldering myeloma | | 1 | | 1 |